

NOVEL SENSING SCHEME FOR A SIX DEGREE-OF-FREEDOM PRECISION POINTING MAGNETIC ACTUATOR

Zhaohui Ren, Lyndon S. Stephens

University of Kentucky, Bearings and Seals Laboratory
Department of Mechanical Engineering, 151 RGAN, Lexington, KY 40506
zren0@enr.uky.edu, stephens@enr.uky.edu,

David J. Carroll

Airex Corporation
Route 108, Dover, NH 03820
dcarroll@airex.com

ABSTRACT

A novel six degree-of-freedom (DOF) prototype gimbal system is constructed to demonstrate the new gimbals for space laser communication applications. The precision pointing magnetic actuator is essentially an open loop unstable system, feedback control is therefore indispensable. To realize ultra-fine pointing accuracy over relatively large gimbal angles, the sensing scheme is critical for the actuator performance. To provide high resolution and contact free feedback for several functions simultaneously at a minimal cost, a novel sensing strategy that uses a tape encoder and hall effect probe arrangement is proposed. In this paper, the prototype gimbal system is introduced and the requirements for the feedback devices are analyzed first. The sensing scheme is presented and its decoding logic is explained. Issues involved in this scheme are discussed. Finally, the proposed sensing scheme is validated by experimental results.

INTRODUCTION

Gimbals with precision pointing functionality in space applications currently employ mechanical bearings. Advances in electromagnetic suspension and electronic drive technology point the way for new gimbals with higher pointing accuracy, increased reliability, vibration isolation capability, lower weight and reduced power dissipation, lubricant free operation and longer functional life. Instead of having separate active magnetic bearing (AMB) and motor components, integral motor-bearings using a single electromagnetic actuator to perform both the bearing and motoring functions, ushers in the next generation of gimbals with higher stiffness, pointing accuracy and power density.

A new permanent magnet (PM) self-bearing motor (SBM) design [1-5] eliminates the trade-off between torque and bearing force production and the stator teeth that can saturate and limit peak torque shown in other designs [6,7]. The slotless construction allows for a smoother torque production, making it beneficial for precision pointing and smooth angular slewing

applications. To evaluate the characteristics of the precision pointing actuator, an optical tracker test rig is constructed for laser communication applications. This novel six DOF magnetic actuator incorporates two slotless SBMs to produce both radial bearing forces and motoring torque simultaneously and one conventional thrust AMB to provide axial support.

Previous work [1] has shown that the slotless SBM and its associated control are able to point down to the resolution of the feedback devices, sensor performance is thus a limiting factor in the performance capability of the actuator. In AMB applications, it's a common practice to have separate sensors for each axis [5], where eddy current probes are used for radial and rotary encoder for angular displacement measurements. Because the 6-DOF actuator is completely magnetically suspended and driven, all the positional feedback devices have to be non-contacting. While the axial sensing is relatively easy to implement, the radial/angular feedback requirements represent a potential inability to demonstrate the gimbal. To provide high resolution and contact free feedback for several functions simultaneously at a minimal cost, a novel sensing strategy based on tape encoders is proposed [8]. Its working principle is discussed and verified by experimental evaluation. Therefore, the proposed sensing scheme is concluded to be satisfactory for the desired performance requirements.

NOMENCLATURE

L_t	Total length of the shaft
R_s	Outer radius of the sensor plate
Res_{ang}/Res_{lin}	Encoder angular/linear resolution
$V_{sx,t}/x_b, V_{sy,t}/y_t$	Decoded/actual top x, y displacement
$V_{sx,b}/x_b, V_{sy,b}/y_b$	Decoded/actual bottom x, y displacement
$V_{s\theta}/\theta, V_{sz}/z$	Decoded/actual θ, z displacement
$V_{s\alpha}/\alpha, V_{s\beta}/\beta$	Decoded/actual α, β displacement
$e_{SL1}, e_{SL2}, e_{SL3}, e_{SL4}$	Lower encoder or output signal
$e_{SU1}, e_{SU2}, e_{SU3}, e_{SU4}$	Upper encoder or output signal
$h_{SL1}, h_{SL2}, h_{SL3}, h_{SL4}$	Lower hall effect probe or signal
$h_{SU1}, h_{SU2}, h_{SU3}, h_{SU4}$	Upper hall effect probe or signal

TEST RIG DESCRIPTION

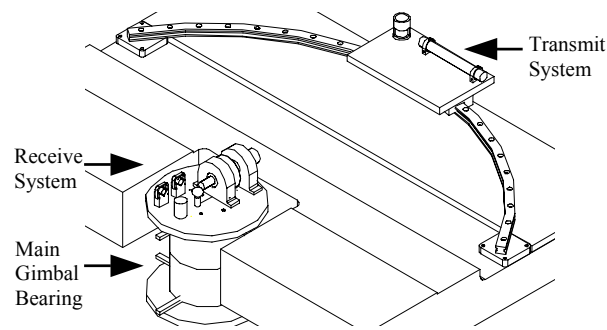


Figure 1. Optical tracker test rig layout

As shown in Fig. 1, the optical tracker test rig uses laser communication as a premise to demonstrate the precision pointing gimbal. It consists of a transmit system, a receive system and the main gimbal bearing (MGB) that incorporates state of the art slotless SBM technology.

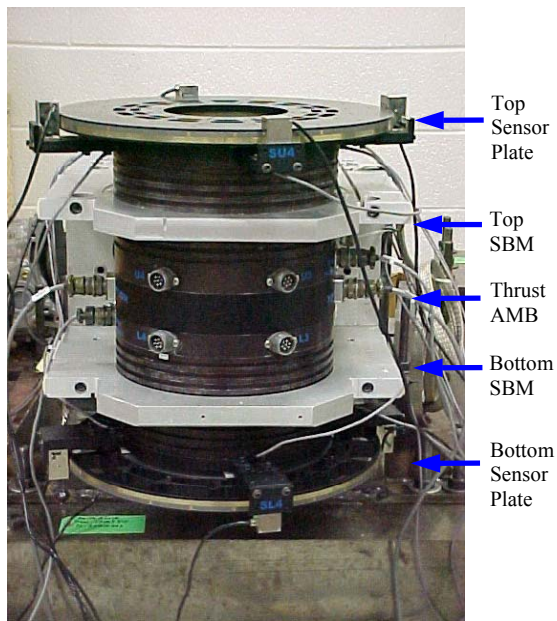


Figure 2. MGB on the test stand

The transmit system includes a laser source traveling along a 45° curved track. The receive system consists of an optical bench mounted to the MGB rotor with such optical components as telescope, mirrors, etc. Fig. 2 is an overview of the MGB, consisting of two slotless SBMs with a thrust AMB in between, one sensor plate being targeted by four encoder read heads and four hall effect probes (90° apart) at each end. For scale, the sensor plates are 16 inches in diameter, the black housings are 11 inches in diameter, and the height of the system is about 17.5 inches. A close up of the

incremental tape based linear sensor arrangement is shown in Fig. 3.

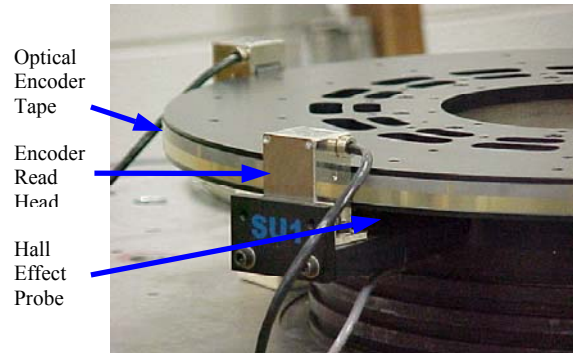


Figure 3. Close up of the MGB sensors

SENSING SCHEME

Fig. 4 shows the systematic diagram of the MGB along with the proposed sensing scheme. Each SBM has PM poles attached circumferentially to the outer diameter of the cylindrical rotor and windings attached to the inner diameter of the slotless stator back iron. The thrust AMB utilized at the mid-span of the rotor is a typical cylindrical Maxwell type AMB with a separate stator winding on each side of a rotor mounted thrust disk. Each sensor plate has a linear reflective metal tape wrapped around its outer diameter and is surrounded by four encoder read heads. Additionally, four hall effect probe assemblies including PMs are mounted axially offset from a ferromagnetic ring mounted to the underside of each sensor plate. The laser shown in Fig. 4 illustrates the received laser beam by the receive system coming from the laser source sent by the transmit system, as shown in Fig. 1.

The MGB rotor is treated as a rigid body and has four types of basic movements, as depicted in Fig. 5. Azimuth is the rotation along a horizontal plane. Elevation is the tilting relative to the normal position of a horizontal plane. Radial offset or eccentricity indicates how the rotor is positioned radially in the horizontal direction. Thrust motion shows how the rotor is positioned axially in the vertical direction. All these motions are required for either tracking and pointing or the rotor stabilization within the clearance air gap. Therefore, the levitated MGB has totally 6 DOF, all of which require feedback for control purpose. The linear tape encoding and hall effect probe sensing strategy is employed for the four types of motions and six DOF.

Angular and Radial Sensing Scheme

Angular and radial displacement measurements at each SBM are necessary and sufficient to identify the azimuth, radial and elevation motions of the MGB rotor. It represents the most challenging task in the whole feedback system. A group of eight optical

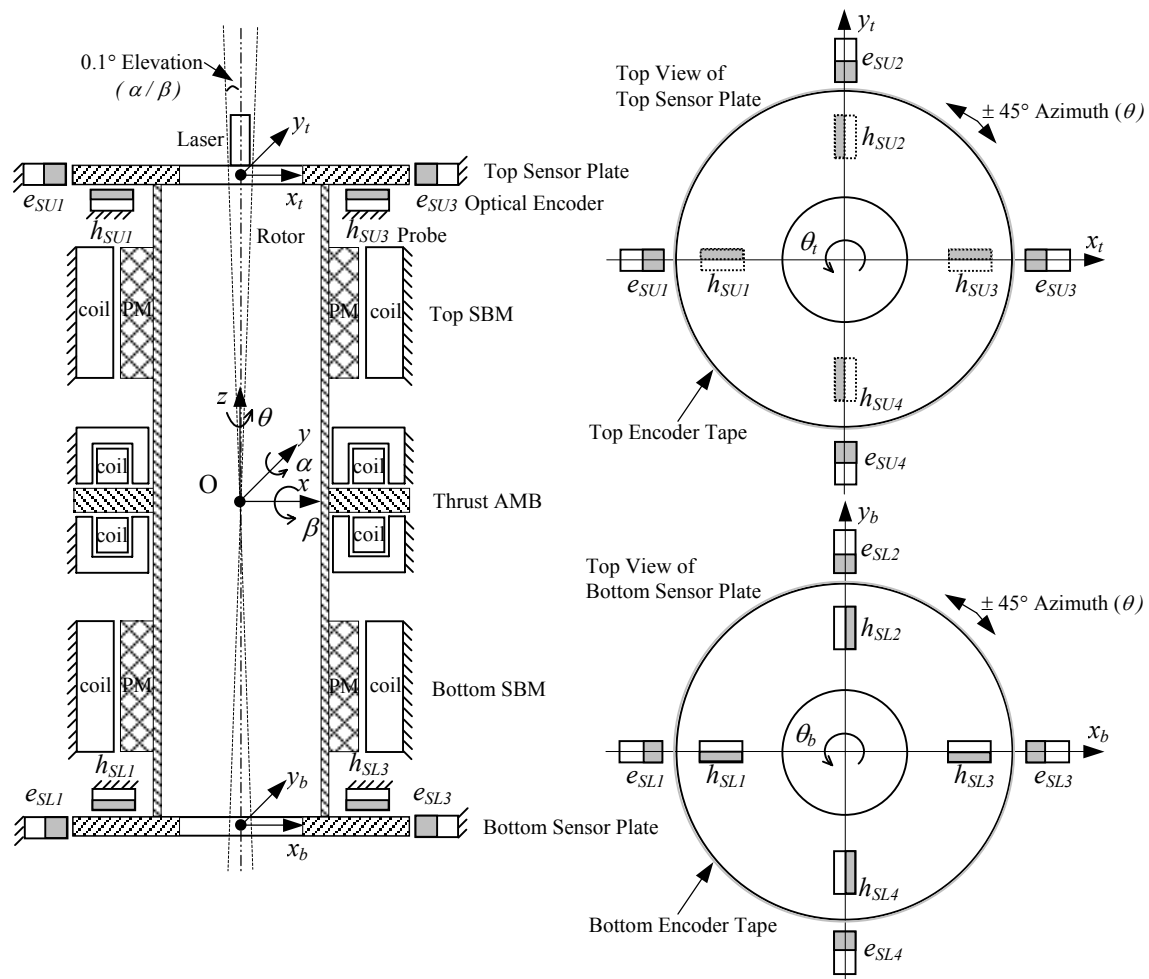


Figure 4. MGB layout with the proposed sensing scheme

incremental encoders are arrayed to work together to measure the angular and radial positions at both upper and lower SBMs simultaneously, as shown in Figs. 2-4.

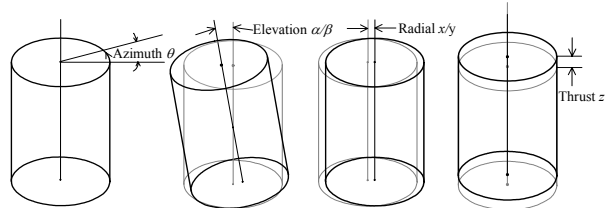


Figure 5. Basic movements of the MGB rotor

The main concern for this non-contact tape encoder system is how to maintain the desired resolution for accuracy, with the large radial clearance gap in which the rotor can move eccentrically about and the rotor radial/axial motion. Detailed tests were performed for a number of gaps, elevations and skew angles of the encoder read head relative to the line direction of the incremental tape. A horizontal milling machine equipped with a rotary table was used to provide precise test alignment between a short sample of a linear tape scale with 100-micron pitch and a MS 50-30 analog output read head by RSF Electronics. The read

head was mounted to the upright of the milling machine. The tape strip was wrapped on the edge of a 16" diameter circular plate mounted on the rotary table. As the rotary table was spun, the read head produced a sinusoidal output changing with the positions. The voltage outputs of both "A" and "B" channels were measured with an oscilloscope. The peak-to-peak voltages were gathered for varying read head to tape positions. The test data was extrapolated to both analog and digital units and used along with various manufacturers' data to select the appropriate tape resolution and read head features for use in the magnetic bearing pointing system. For most commercially available alternatives, the gap between the read head and tape scale is usually small and does not allow for variation. A RSF MS55-45M digital output linear encoder with 200-micron pitch is chosen because of its high linear resolution, high electrical/sensing bandwidth and large range of allowable clearance gap between read head and tape.

Axial Thrust Sensing Scheme

Thrust position measurement is straightforward. Hall effect probes are chosen because they provide

adequate resolution and a linear output-to-position signal, are compact in size, readily available and relatively inexpensive. Refer to Figs. 2-4, four probes are positioned 90° apart at each end of the stator, because both the rotor and endplates are hollow and elevation may couple with the thrust motion. Each hall effect probe consists of a hall sensor attached in the center of a small rectangular iron plate, two round button type PMs attached to the plate near its edges along the centerline of the larger dimension. The magnets are positioned with their “North” faces toward the plate. Thus each sensor assembly produces a nearly linear response to the presence of a nearby ferromagnetic object. The Micronas HAL400S-C hall sensor is chosen, because it produces a differential output signal that compensates for thermal drift in the sensor and cancels common mode electrical noise. This results in an even more compact overall assembly size.

DECODING LOGIC

The output signals from all the sensors are fed into a digital controller via a counter interface for the encoder channels, buffer and ADC for the hall probes, and manipulated to produce the desired positional measurements, based on the principles discussed below.

Thrust Probe Network

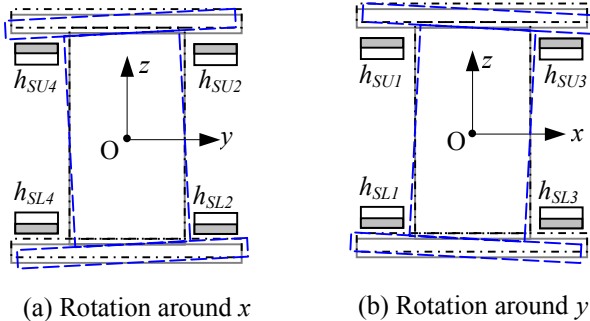


Figure 6. Hall probe system working principle

The eight hall effect probe signals are biased and scaled into a uniform output range within the limit of rotor axial travel. As shown in Fig. 6, the four probes in y - z plane form a rectangle with two diagonals from h_{SU2} to h_{SL4} and h_{SU4} to h_{SL2} . Similarly, the four in x - z plane form another rectangle with two diagonals from h_{SU1} to h_{SL3} and h_{SU3} to h_{SL1} . When the rotor is straight and centered axially (solid), the eight hall effect probes produce exactly the same readings, the axial position of the rotor should be zero. If the rotor is straight but bounced a distance d in z direction (dash-dotted), the lower and upper sets of probes would see the same amount of change in readings but of opposite sign, the rotor axial position corresponds to d . If the rotor is tilted in one plane (dashed), the four on the same plane

would experience the same change in readings with two diagonals of opposite sign, but the four on the other plane won't see any difference, the rotor axial position should be zero.

Eq. (1) is applicable to any combination of the above cases to produce the rotor displacement in z direction from the probe outputs. Obviously, the redundant sensor configuration allows for better accuracy and fault tolerance.

$$V_z = \frac{\frac{h_{SL1} - h_{SU3}}{2} + \frac{h_{SL2} - h_{SU4}}{2} + \frac{h_{SL3} - h_{SU1}}{2} + \frac{h_{SL4} - h_{SU2}}{2}}{4} \quad (1)$$

Angular/Radial Encoder Network

For each set of four encoders reading the same tape wrapped around one sensor plate, two encoders positioned directly opposite from each other could determine if the plate movement relative to them is radial, angular or both. As illustrated in Fig. 7, if both e_{SL1} and e_{SL3} read a change of the same counts, the bottom plate is rotated in θ direction. If e_{SL3} reads an increase but e_{SL1} reads a decrease of the same counts, a pure radial movement in y direction occurs. If changes are not of equal magnitude, there is a combination of radial and rotational movements. Same rules apply for all the other pairs of encoders. In Fig. 7, the solid circle stands for the centered plate, dashed represents the plate displaced by dx in x direction, and dash-dotted is after the plate moves a distance dy in y direction.

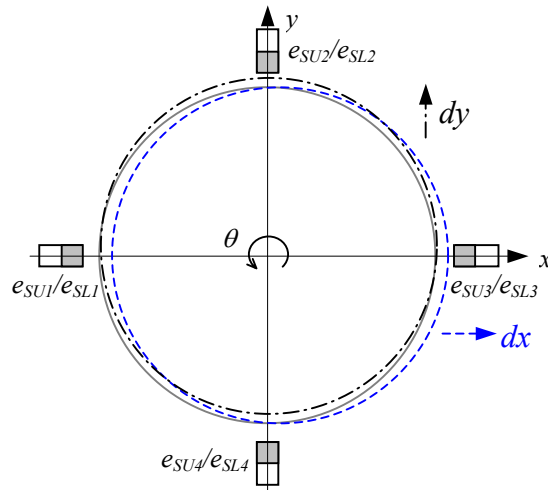


Figure 7. Encoder system working principle

The decoded top x and y , bottom x and y , and angular θ displacements of the rotor can be calculated using Eq. (2) from the eight encoder readings. Since the upper encoder set is facing oppositely to the lower set, when the rotor is rotated clockwise, the upper set would read an increase in counts, but the lower set would read a decrease in counts, and vice versa.

$$\begin{aligned}
 V_{sx,t} &= \frac{e_{SU2} - e_{SU4}}{2} \cdot Res_{lin}, & V_{sy,t} &= \frac{e_{SU1} - e_{SU3}}{2} \cdot Res_{lin} \\
 V_{sx,b} &= \frac{e_{SL4} - e_{SL2}}{2} \cdot Res_{lin}, & V_{sy,b} &= \frac{e_{SL3} - e_{SL1}}{2} \cdot Res_{lin} \\
 V_{s\theta} &= \frac{\frac{e_{SU1} + e_{SU2} + e_{SU3} + e_{SU4}}{4} + \frac{e_{SL1} + e_{SL2} + e_{SL3} + e_{SL4}}{4}}{2} \cdot Res_{ang}
 \end{aligned} \quad (2)$$

Eq. (2) is applicable to any combination of radial and rotational movements. When all the eight encoders are necessary for the desired radial feedback requirements, θ measurement possesses the greatest redundancy. This redundancy further increases the angular resolution offered by each individual encoder, beneficial for the precision pointing system. Refer to Fig. 4, the pointing angle α/β around y/x axis is calculated as:

$$V_{s\alpha} = \arctg\left(\frac{V_{sx,t} - V_{sx,b}}{L_t}\right), \quad V_{s\beta} = \arctg\left(\frac{V_{sy,b} - V_{sy,t}}{L_t}\right) \quad (3)$$

ISSUES INVOLVED IN THE ENCODER SYSTEM

One problem experienced with the tape encoder system during experiments is initialization. Whenever the controller is restarted, the incremental encoder readings would begin with 0 no matter where the rotor resides. Eq. (2) would give 0 in all the five DOF, corresponding to the rotor at the desired angular home position and centered radially at both ends, but it most certainly is not the case in reality as magnetic bearing systems are open loop unstable. Therefore a mechanism to determine the initial rotor position and compensate the initial encoder readings has to be provided for the system to function properly. A desired angular position can be marked as home position and started with each time. One solution for the radial part is to apply open loop forces at both SBMs first, to enforce the rotor always start at a known position, such as that against one side of the radial backup bearings at both ends, once the system is restarted. Then encoder readings can be corrected inside the controller to correspond to that position, before the feedback controller takes over. Still another option is to provide index markings on the incremental encoder tape that act as home positions (the present system does not have these index marks). The open loop forces would then be applied to the actuators to drive the rotor to the home position and all sensor readings will be relative to that position. The addition of the index pulses would also provide signals during operation that may be used to correct for missed counts, resulting in increased accuracy. Another solution to the startup problem is to use an absolute type tape encoder. However, the lower resolution given the required radial travel prohibit the use of this solution for this experiment.

As illustrated in Fig. 7, when the top (bottom) plate moves in x , or y direction, encoders e_{SU2} and e_{SU4} (e_{SL2} and e_{SL4}), or e_{SU3} and e_{SU1} (e_{SL3} and e_{SL1}) see a same amount of change in counts but of opposite sign. When the rotor rotates, all the eight encoders experience the same amount of change in counts, but the top and bottom four change in opposite directions. The following mapping from the rotor positions to the encoder readings results:

$$\underbrace{\begin{Bmatrix} e_{SU1} \\ e_{SU2} \\ e_{SU3} \\ e_{SU4} \\ e_{SL1} \\ e_{SL2} \\ e_{SL3} \\ e_{SL4} \end{Bmatrix}}_{[M]} = \frac{1}{Res_{lin}} \begin{bmatrix} 1 & -R_s & & & & & & \\ & 1 & -R_s & & & & & \\ & & -1 & -R_s & & & & \\ & & & -1 & -R_s & & & \\ & & & & R_s & & -1 & \\ & & & & R_s & & -1 & \\ & & & & R_s & & & 1 \\ & & & & R_s & & & 1 \end{bmatrix} \begin{Bmatrix} V_{sx,t} \\ V_{sy,t} \\ V_{s\theta} \\ V_{sx,b} \\ V_{sy,b} \end{Bmatrix} \quad (4)$$

The mapping matrix $[M]$ can be used for initial encoder reading correction. On the other hand, the rotor positions at any time can also be determined from the eight encoder readings by means of the Moore-Penrose pseudo inverse $[M^+]$ of $[M]$, with T being the transpose.

$$[M^+] = [M]^T \left([M][M]^T \right)^{-1} \quad (5)$$

It can be shown that $[M^+]$ is equivalent to the proposed decoding logic in Eq. (2). The angular/radial encoder sensing scheme is thus invertible and provides a one-to-one correspondence between the encoder reading and rotor position vectors.

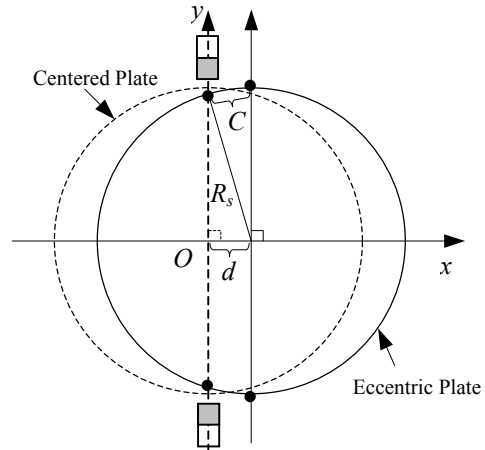


Figure 8. Approximation in the radial measurement

As illustrated in Fig. 8, when the circular plate with tape passes by the encoder read heads, what the read heads really see is not the linear radial displacement, but the curved arcs. Eqs. (2) and (4) approximate the

desired linear radial displacements by curved arcs seen by encoder read heads. Eq. (6) gives the error induced from this approximation, where d is the actual radial displacement, C is its arc approximation.

$$e = \frac{C-d}{d} \times 100\%, \quad C = R_s \left[\frac{\pi}{2} - \arccos\left(\frac{d}{R_s}\right) \right] \quad (6)$$

When the plate moves from one side of the radial air gap all the way to the other, e reaches its maximal calculated value of $4e-4\%$, which is negligible and thus the radial positional measurements are very accurate.

As shown in Fig. 9, there exists a discontinuity in the metal tape glued to the outer diameter of each plate. If the discontinuity is sufficiently large, whenever the gap passes by an encoder read head, a significant number of counts are missing from that encoder. The $\pm 45^\circ$ azimuth requirement of this system allows to avoid such gap passes. When the existing system is used with angular travels exceeding 90° , care should be taken to match the encoder pitch thus maintain the line spacing at the discontinuity and compensate such losses. The effects of the tape gaps on sensing accuracy without alignment of lines as is and any compensation mechanism are discussed in the next section.

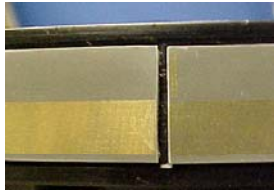


Figure 9. Encoder tape gap

EXPERIMENTAL EVALUATION

The premise of the tape encoder system is that the read head literally reads its position along the linear tape scale. By wrapping the scale around the cylindrical plate, that linear position is easily transformed to an angular position. The linear resolution of the encoder is $1\mu\text{m}$, so its theoretical angular resolution is:

$$Res_{ang} = \frac{Res_{lin}}{R_s} = \frac{1\mu\text{m}}{(8\text{in} + 0.8\text{mm})} = 4.90\mu\text{rad} \quad (7)$$

By manually rotating the rotor for a certain angle and averaging the corresponding count changes of the eight encoders, the angular resolution is experimentally determined to be approximately $4.96\mu\text{rad}$.

Experiments are carried out to evaluate the angular/radial encoder scheme. Since precision pointing is a key feature of the system, measuring accuracy of the rotational movement plays the most important role on the system performance. The first set of experiments

is to verify that the decoded $V_{s\theta}$ from Eq. (2) truly indicates the actual angular displacement θ . The rotor is manually rotated for $1/16$ revolution each time, the estimated θ and corresponding $V_{s\theta}$ are recorded. In Fig. 10, the solid line having a slope of 1 deg/deg is desirable with $V_{s\theta}$ and θ perfectly matching each other, solid data points are taken for the counterclockwise rotation up to 360° , and hollow ones clockwise back to 0° . Surprisingly, the data shows good agreement, accuracy, linearity and repeatability, even with the crude test method. Also notice that the collected data points are not perfectly located on the desired line, the closer the solid point is towards 360° the further below the desired point, the closer the hollow point towards 0° the further above the desired point. The slope of the best fit line (not shown in Fig. 10) is 0.9902 deg/deg , deviated from the desired value by 0.98% .

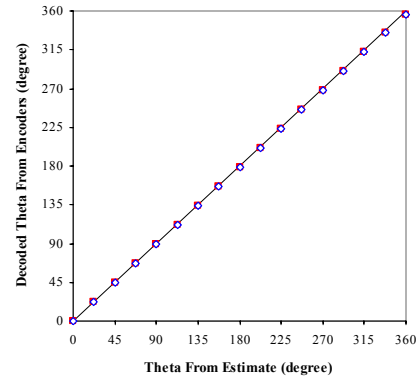


Figure 10. $V_{s\theta}$ VS. θ

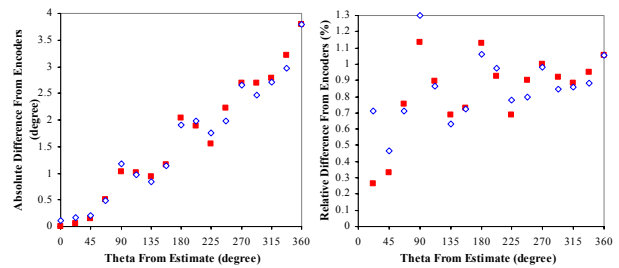


Figure 11. $E_{s\theta}$ VS. θ and $E_{s\theta}/\theta$ VS. θ

To identify the source, absolute and relative differences are shown in Fig. 11. In both plots, on the way up to 360° a local maximum occurs every 90° , exactly when each tape gap passes by one of the four read heads around each plate. Therefore tape gaps contribute the difference most significantly. Each such pass causes two out of eight more encoder readings corrupted, a local maximum results, and the difference is averaged out partially right after the pass and then increases again due to the accumulation. At the end of full 360° excursion all the encoder readings are corrupted, the absolute difference reaches its global

maximum 3.80°. On the way back to 0°, starting at 337.5° one pass occurs again every 90°, this count loss partly compensates the previous difference at the same location and makes the data point closer to its desired one, so hollow points are always lower than the solid ones at these locations. Relative difference reaches its global maximum 1.30% at 90° on the way back.

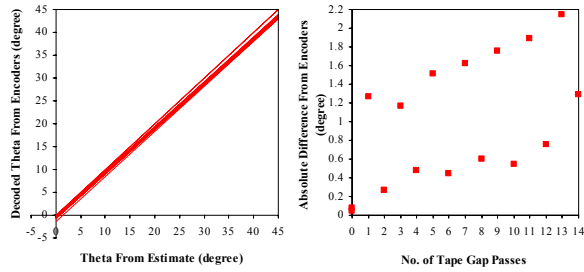


Figure 12. Effects of tape gaps

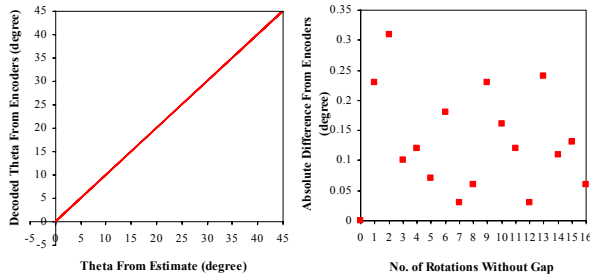


Figure 13. Repeated rotation without gap

To further investigate how the tape gaps affect accuracy, a set of data is collected when the rotor is rotated back and forth between 0° and 45° with tape gaps in between, the results are shown in Fig. 12. As expected, as the number of passes increases, the decoded signal is further away from 0° and 45°. Test results with rotor rotating between 0° and 45° but no gap in between are shown in Fig. 13, difference is clearly reduced significantly compared to Fig. 12. Since the optics in each read head use an average of at least 10 encoder lines a pre-made tape with a gap less than 3 lines would allow sensing over large excursion angles. For applications where a pre-made unit is not available and the total rotational excursion exceeds 90°, if the accuracy compromise due to the large discontinuity is not acceptable, a compensating scheme has to be applied to the encoder readings.

Similar experiments are intended to validate the radial motion sensing scheme. Top or bottom SBM coils are energized to generate open loop radial forces to move the rotor back and forth radially against sides, meanwhile different shims are applied inside the radial clearance gap to limit the total movement allowed, and a dial indicator is located next to a encoder read head aligned with the motion axis. After each movement, the

dial indicator readings and encoder results are recorded. Figs. 14 and 15 show the results for bottom x and top y movement respectively, where the solid line having a slope of 1 mil/mil is desirable with $V_{sx,b}$ and x_b or $V_{sy,t}$ and y_t perfectly matching each other, solid and hollow data points are taken with dial indicator located at either side of the encoder read head, the dashed line best fits the two data sets by averaging the two best fit lines.

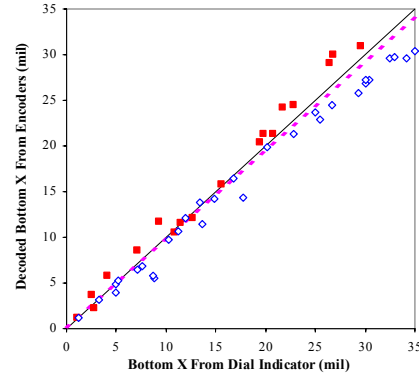


Figure 14. $V_{sx,b}$ VS. x_b

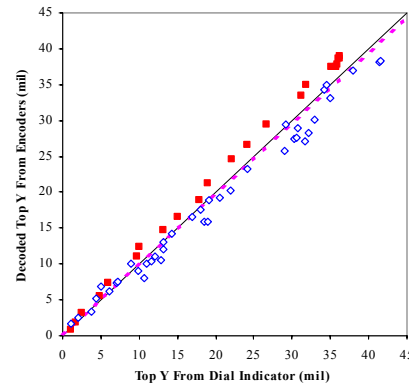


Figure 15. $V_{sy,t}$ VS. y_t

In both plots, the dashed line is very close to the solid one, which clearly shows the decoded signal truly depicts the appropriate radial motion. Specifically, the slope of the dashed line, 0.9789 mil/mil for bottom x and 0.9887 mil/mil for top y , is different from the desired value only by 2.11% and 1.13% respectively, therefore the performance of the radial sensing scheme is satisfactory. Also notice that the two data sets scatter on either side of the desired line, and the overall trend is the larger movement, the bigger difference. This is due to the inherent problem with the experimental setup. The actual rotor motion inside the radial and thrust clearance gap can be very complicated, but the dial indicator can't be located at exactly the same location as the encoder read head. Even though the radial force is applied, it's not guaranteed that the rotor actually moves perfectly along the intended axis, non-collocation between the encoder and dial indicator

along the cylindrical plate would then very possibly cause one data set from encoders always higher than the dial indicator readings, but the other set lower.

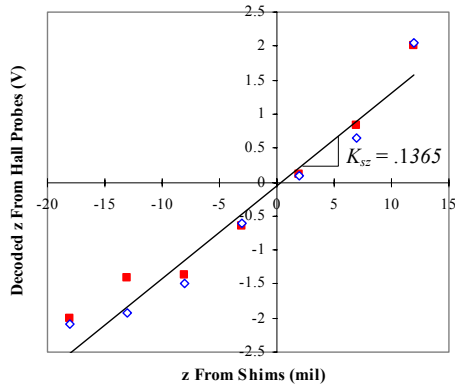


Figure 16. V_{sz} VS. z

The final experiment carried out evaluates the thrust hall effect probe scheme. The thrust clearance gap is shimmed differently to limit the total axial movement, top or bottom thrust coils are energized to pull the rotor up or push it down, the z displacement from shims and its corresponding decoded V_{sz} from Eq. (1) are recorded and shown in Fig. 16. Solid line is the best fit line, solid data points are collected from bottom up and hollow ones from top down. The data shows good linearity and repeatability. Sensitivity for the hall effect probe system is determined to be 136.5 V/in.

The performance of the proposed sensing scheme for feedback control purpose of the six DOF magnetic actuator, as discussed above, is summarized in Table 1.

Table 1. Feedback performance summary

	Property	Symbol	Unit	Value
Theoretical	Linear resolution per encoder	Res_{lin}	μm	1
	Angular resolution per encoder	Res_{ang}	μrad	4.90
	Max. error in linear approximation by arc	e	%	4e-4
Experimental	Angular resolution	$Res_{ang-exp}$	μrad	4.96
	Sensitivity $V_{s\theta}/\theta$ for θ ($0^\circ \rightarrow 360^\circ \rightarrow 0^\circ$)	$K_{s\theta}$	deg/deg	0.9902
	Relative difference in $K_{s\theta}$ ($0^\circ \rightarrow 360^\circ \rightarrow 0^\circ$)	$(K_{s\theta}-1)/1$	%	0.98
	Max. absolute difference in $V_{s\theta}$ ($0^\circ \rightarrow 360^\circ \rightarrow 0^\circ$)	$E_{s\theta}$	deg	3.80
	Max. relative difference in $V_{s\theta}$ ($0^\circ \rightarrow 360^\circ \rightarrow 0^\circ$)	$E_{s\theta}/\theta$	%	1.30
	Max. absolute difference in $V_{s\theta}$ ($0^\circ \leftrightarrow 45^\circ$ with 14 gap passes)	$E_{s\theta-gap}$	deg	2.14
	Max. absolute difference in $V_{s\theta}$ ($16\ 0^\circ \leftrightarrow 45^\circ$ with no gap pass)	$E_{s\theta-nogap}$	deg	0.31
	Sensitivity $V_{sx,b}/x_b$ for bottom x	$K_{sx,b}$	mil/mil	0.9789
	Relative difference in $K_{sx,b}$	$(K_{sx,b}-1)/1$	%	2.11
	Sensitivity $V_{sy,t}/y_t$ for top y	$K_{sy,t}$	mil/mil	0.9887
	Relative difference in $K_{sy,t}$	$(K_{sy,t}-1)/1$	%	1.13
	Sensitivity V_{sz}/z for z	K_{sz}	V/in	136.5

CONCLUSION

A novel sensing strategy is proposed and applied to a six DOF electromagnetic gimbal prototype system. The unique combination feedback technology combines the sensing functions for the angular and radial motions of the rotor, thus eliminating the need for additional radial position probes. The experimental results presented in this paper prove that this sensing scheme results in a workable feedback system and is adequate for the test rig demonstration. Such a combined angular and radial sensing strategy has potential applications in combined magnetic motor bearings and other precision contactless angular and radial positional measurements. The remaining challenge for this system is the estimate of the initial position at startup.

ACKNOWLEDGMENTS

The authors express their appreciation to Airex Corporation of Dover, NH, USA, for partial sponsorship of this research.

REFERENCES

- [1] Carroll, D., Sedgewick, J., and Stephens, L.S., 1999, "Long life, fault tolerant, spacecraft sensor gimbal/bearing system final report," United States Air Force Research Laboratory/VSDV, Contract No. F29601-98-C-0188.
- [2] Stephens, L.S., and Kim, D.G., 2001, "Analysis and simulation of a Lorentz-type, slotless self-bearing motor," IFAC Journal of Control Engineering Practice, July, pp.899-905.
- [3] Stephens, L.S., and Kim, D.G., 2002, "Force and torque characteristics for a slotless, Lorentz self bearing servomotor," IEEE Transactions on Magnetics, 38, pp.1764-1773.
- [4] Kim, D.G. and Stephens, L.S., 2000, "Fault tolerance of a Lorentz-type self bearing motor according to the coiling schemes," Proc. 7th Int. Symp. Magn. Bearings, ETH, Zurich, Switzerland, pp.219-224.
- [5] Steele, B.A. and Stephens, L.S., 2000, "A test rig for measuring force and torque production in a Lorentz, slotless self bearing motor," Proc. 7th Int. Symp. Magn. Bearings, ETH, Zurich, Switzerland, pp.407-412.
- [6] Chiba, A., Rahman, M.A., and Fukao, T., 1991, "Radial forces in bearingless reluctance motor," IEEE Transactions on Magnetics, 27, p. 786.
- [7] Okada, Y., Konishi, H., Kanebako, H., and Lee, C.W., 2000, "Lorentz force type self bearing motor," Proc. 7th Int. Symp. Magn. Bearings, Zurich, pp.353-358.
- [8] Carroll, D., 2002, "Integrated angular & radial position sensor," United States Patent Application No. 60/369,931 Pending, Airex Corporation, NH.